# Advanced Concentration Gradient Cathode Material with Two-Slope for High-Energy and Safe Lithium Batteries

*Byung-Beom Lim, Sung-Jun Yoon, Kang-Joon Park, Chong S. Yoon, Sung-Jin Kim, Juhyon J. Lee, and Yang-Kook Sun**

**$Li[Ni_{0.65}Co_{0.13}Mn_{0.22}]O_2$ cathode with two-sloped full concentration gradient (TSFCG), maximizing the Ni content in the inner part of the particle and the Mn content near the particle surface, is synthesized via a specially designed batch-type reactor. The cathode delivers a discharge capacity of 200 mAh $g^{-1}$ (4.3 V cutoff) with excellent capacity retention of 88% after 1500 cycles in a full-cell configuration. Overall electrochemical performance of the TSFCG cathode is benchmarked against conventional cathode (CC) with same composition and commercially available $Li[Ni_{0.8}Co_{0.15}Al_{0.05}]O_2$ (NCA). The TSFCG cathode exhibits the best cycling stability, rate capability, and thermal stability of the three electrodes. Transmission electron microscopy analysis of the cycled TSFCG, CC, and NCA cathodes shows that the TSFCG electrode maintains both its mechanical and structural integrity whereas the NCA electrode nearly pulverizes due to the strain during cycling.**

## 1. Introduction

Computing and telecommunication devices, ubiquitously present in today's mobile society, have driven the ever-increasing demands for light portable power sources with large capacity. In addition, as a consequence of shortage of fossil fuels, development of electrified automobiles such as plug-in hybrid electric vehicles and electric vehicles (EVs) has further raised the performance requirements of rechargeable battery system. Although lithium-ion batteries (LIBs) are the standard choice for powering mobile electronics, successful use of LIBs in the automotive sector requires significant improvements in energy density, cycle life, and safety characteristics. The research and development efforts in meeting these challenges have focused on identifying and designing new cathode materials with capacity higher than 200 mAh $g^{-1}$ and improved safety characteristics. Two promising candidate cathode materials are $Li[Ni_{0.8}Co_{0.1}Mn_{0.1}]O_2$ (Ni-rich NCM) and $Li[Ni_{0.8}Co_{0.15}Al_{0.05}]O_2$ (NCA), which have been studied extensively for the past decade.[1–3] In fact, Tesla Motors recently disclosed the use of NCA cathode in their 18650-type battery cells as the power unit in their pure EVs with one-charge driving range of 270 miles.[4] Even though Ni-rich NCM and NCA cathodes can potentially deliver capacity as high as 200 mAh $g^{-1}$ (at 4.3 V cutoff voltage), their poor thermal and cycling stabilities are still important issues that need to be addressed.[5,6] If Ni-rich NCM and NCA cathodes are charged to high voltages to obtain higher capacity, abundance of unstable $Ni^{4+}$ ions are formed in the cathodes and tend to be reduced to form stable and insulating NiO phase on the cathode surface, resulting in increased interfacial impedance and consequently poor cycle life.[5,7–9] Concurrently, the reduction of $Ni^{4+}$ to $Ni^{2+}$ in the Ni-rich NCM and NCA cathodes is accompanied by oxygen release, giving rise to poor thermal behavior and safety issues triggered by the reaction with the flammable electrolyte.[5,10,11]

In order to improve the thermal and structural stability of the Ni-rich layered cathode materials, cathodes enriched in Mn at the outer layer were proposed to suppress the undesired $Ni^{4+}$ reduction because $Mn^{4+}$ is naturally stable ($MnO_2$ is a stable compound)[12] and does not participate in the redox reaction during the charge and discharge cycle.[13,14] Recently, we developed a high-energy cathode material with full concentration gradient (FCG) materials (single slope), in which the Ni concentration decreases and the Mn concentration increases linearly toward the particle surface.[15–17] The concentration gradient assures smooth transition from the surface to the bulk and enables the FCG cathode to take advantage of high capacity delivered by the Ni-enriched core and simultaneously the thermal and cycling stability ensured by the Mn-enriched surface layer. It was demonstrated that the FCG $Li[Ni_{0.75}Co_{0.10}Mn_{0.15}]O_2$ cathode delivered a discharge capacity (200 mAh $g^{-1}$ at 4.3 V cutoff voltage and 0.2 C rate)[15] as high as those of the conventional Ni-rich NCM and NCA cathodes while exhibiting excellent cycle life and thermal safety. Here, we extended the FCG concept and report a new novel $Li[Ni_{0.65}Co_{013}Mn_{0.22}]O_2$ cathode material with two-sloped full concentration gradients

B.-B. Lim, S.-J. Yoon, K.-J. Park, Prof. Y.-K. Sun
Department of Energy Engineering
Hanyang University
Seoul 133-791, South Korea
E-mail: yksun@hanyang.ac.kr
Prof. C. S. Yoon
Department of Materials Science and Engineering
Hanyang University
Seoul 133-791, South Korea
Dr. S.-J. Kim, Dr. J. J. Lee
BMW Group
Petuelring 130, 80788 München, Germany

**DOI: 10.1002/adfm.201501430**

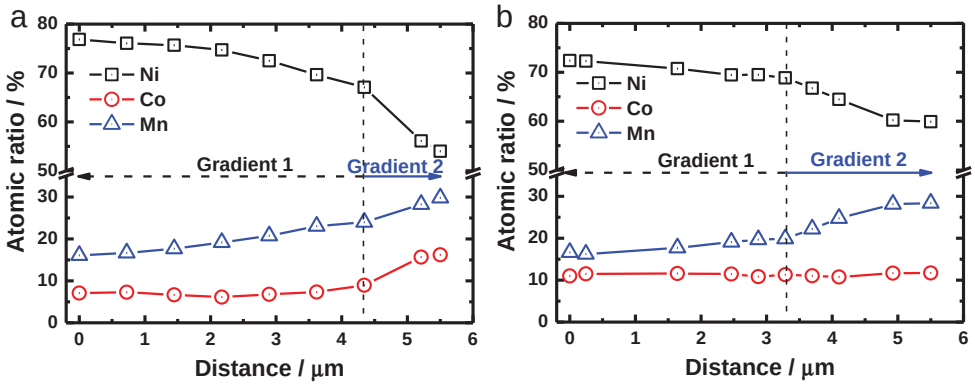


**Figure 1.** EPMA line scan of the integrated atomic ratio of transition metals as a function of the distance from the particle center to the surface for a) the precursor and b) the lithiated TSFCG material.

(TSFCG) of Ni, Co, and Mn ions throughout the cathode particles to maximize the average Ni concentration at the core as active redox species and the Mn concentration in the area near the particle surface. The Ni-rich TSFCG delivers a discharge capacity in excess of 200 mAh $g^{-1}$ (at 4.3 V cutoff voltage and 0.1 C rate) with excellent cycle life and thermal stability. In order to establish the superiority of the TSFCG cathode against the conventional cathodes (CCs), comparison of electrochemical and thermal properties of the TSFCG with those of NCA and CC $Li[Ni_{0.65}Co_{013}Mn_{0.22}]O_2$ (with same average composition of TSFCG) is presented.

## 2. Results and Discussion

Atomic absorption spectroscopy (AAS) was used to determine the average composition of the TSFCG cathode to be $Li[Ni_{0.65}Co_{0.13}Mn_{0.22}]O_2$. To estimate the concentration gradient of each transition metal within a single TSFCG particle, the precursor and lithiated samples were analyzed by electron probe microanalysis (EPMA) with a probe diameter of 1 μm. Relative concentrations of Ni, Co, and Mn were measured across the polished surface of precursor and lithiated particles starting from the particle center. The EPMA data in **Figure 1**a shows the smooth concentration gradients for each transition metal throughout the particle core. The concentration gradients then abruptly changed near the particle surface as designed, confirming that the two-sloped concentration gradients for Ni, Co, and Mn were realized across the precursor particle. The relative compositions of Ni, Co, and Mn concentrations at the center were 77 mol%, 7 mol%, and 16 mol% so that the inner part of the precursor particle was highly enriched in Ni. The Ni concentration gradually decreased while the Co and Mn concentration increased in expense of the reduction of Ni concentration up to ≈4.3 μm from the center, at this point all three concentration gradients sharply changed. Over the next 1.2 μm, the relative composition of Ni reduced from 67 to 54 mol% while the compositions for Co increased from 9 to 16 mol% and for Mn increased from 24 to 30 mol%. Figure 1a clearly evinces that the two-sloped concentration gradients for Ni, Co, and Mn were realized across the precursor particle with highly Ni-enriched inner bulk and significant reduction in Ni concentration at the surface. The lithiation process of the precursor particle caused slight interdiffusion of Ni, Co, and Mn during high-temperature calcination and led to the somewhat flattened gradient (Figure 1b), compared to those of the precursor particle. However, the basic compositional scheme composed of two-sloped concentration gradients for the transition metal ions was well maintained in the lithiated oxide particle (particle center: $Li[Ni_{0.72}Co_{0.11}Mn_{0.17}]O_2$ and surface: $Li[Ni_{0.60}Co_{0.12}Mn_{0.28}]O_2$).

Cross-sectional transmission electron microscopy (TEM) images of the TSFCG particle was obtained by sectioning a single particle using focused ion beam. A cross sectional TEM image (mosaic of several images) in **Figure 2**a shows that the TSFCG particle was mainly composed of elongated primary particles radially emanating from the particle center similar as observed in the FCG particle.[16] While the center of the TSFCG particle consist of 0.5 μm sized equiaxed primary particles with 0.2 μm in width which grew centrally from the particle center as can be seen from Figure 2b. Electron diffraction analysis of the elongated primary particles verified that the primary particles were crystallographically textured such that the layered planes in each primary particle oriented along the radial directions, pointing outward from the center. A similar crystallographic texturing was also observed in the FCG particle.[16] A magnified TEM image of a primary particle and the corresponding high-resolution TEM image taken in the 100 zone are shown in Figure 2c,d. The high-resolution image clearly verified that the 003 planes of the layered structure were aligned such that the planes radiated from the center of the primary particle. In spite of having the concentration slope change, the microstructural advantages of a FCG particle namely, radial alignment of the primary particles and crystallographic texturing were retained in the TSFCG particle.

Electrochemical performance of the TSFCG, CC $Li[Ni_{0.65}Co_{0.13}Mn_{0.22}]O_2$, and NCA $Li[Ni_{0.80}Co_{0.15}Al_{0.05}]O_2$ cathodes was evaluated in both 2032 coin-type half-cells and pouch-type full cells. As shown in **Figure 3**a, the TSFCG delivered a high discharge capacity of 200 mAh $g^{-1}$. In comparison, the NCA cathode showed a slightly reduced capacity of 198 mAh $g^{-1}$ whereas the CC cathode exhibited much lower capacity of 187 mAh $g^{-1}$. Considering the average composition of the redox species of Ni in the TSFCG $Li[Ni_{0.65}Co_{0.13}Mn_{0.22}]O_2$ cathode, the highest capacity obtained from TSFCG is rather

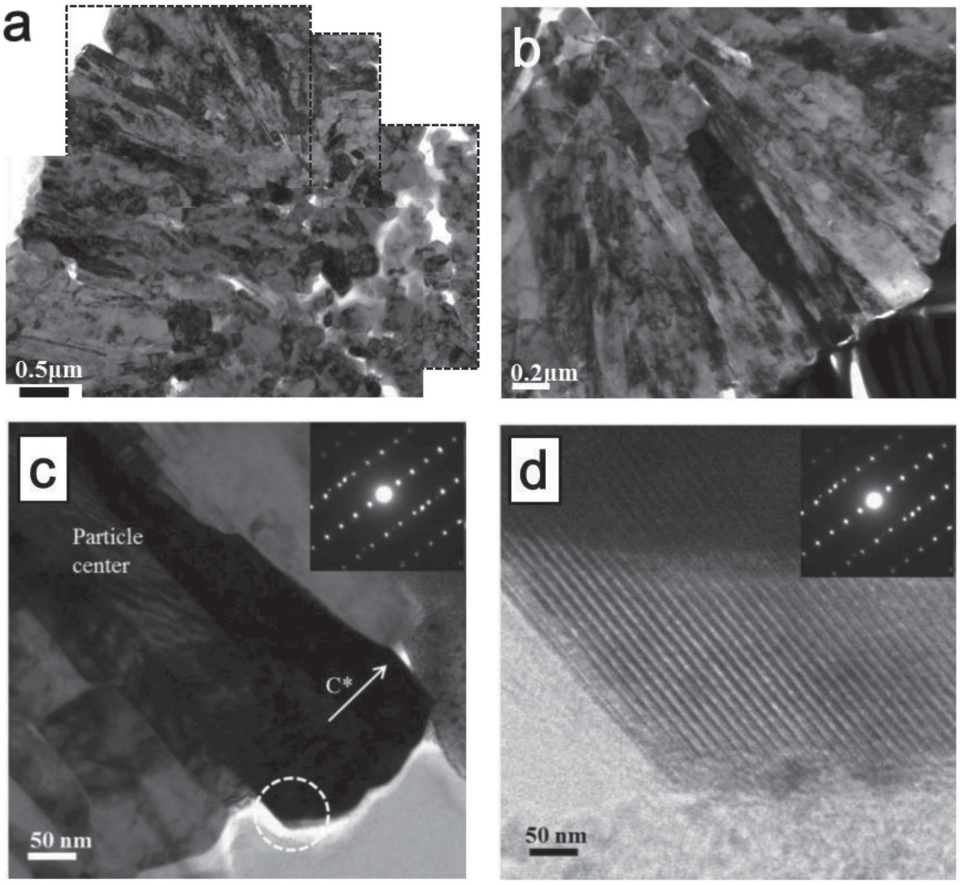


**Figure 2.** a) TEM image (mosaic of several images) of as-prepared TSFCG electrode, illustrating the rod-shaped primary emanating from the equiaxed particles at the particle center, b) a bright field TEM image showing a single elongated primary particle (dark particle at the center of the image), c) a magnified bright field TEM image of a primary particle, and d) corresponding high-resolution TEM image from the marked region in (c) taken in the 100 zone.

unusual. It is believed that the enhanced capacity of the TSFCG cathode was originated from the higher concentration of active $Ni^{2+}$ concentration of TSFCG in the outer particle surface region as the Mn-enriched surface region suppressed the two-electron reaction ($Ni^{2+} \rightarrow Ni^{4+}$) on charging which is one of main advantages of the FCG cathode material.[14,16] Note that the 1st cycle Coloumbic efficiency of the TSFCG cathode was 95.9%, which is much higher than 94.4% of CC and 92.9% of NCA due to the well-developed nanorod-shaped primary particles preferentially grown in the radial directions with crystallographic texture.

To assess the structural stability of TSFCG material, the cells were tested by cycling to 4.3 V at 30 °C under 0.5 C rate (90 mA $g^{-1}$). As seen in Figure 3b, the TSFCG cathode showed excellent capacity retention of 96.6% after 100 cycles, still maintaining a discharge capacity of 182 mAh $g^{-1}$ after 100 cycles whereas the CC and NCA cathodes retained 94.4% and only 90.8% of their initial capacities, respectively. This rapid decrease in capacity for the NCA cathode was mainly ascribed to the reaction of $Ni^{4+}$ at the particle surface with the electrolyte during the high-voltage charging, resulting in structural degradation at cathode particle surface and electrolyte decomposition.[8,15] In contrast, the particle surface of the TSFCG cathode was stabilized by increasing the stable $Mn^{4+}$ concentration at the surface and thus reducing the possibility of the detrimental reaction of the redox species with the electrolyte.[13] In addition, the lower specific surface area of the TSFCG (0.34 $m^2$ $g^{-1}$, pore volume: $1.61 \times 10^{-3}$ cc $g^{-1}$) compared to those of the CC (0.52 $m^2$ $g^{-1}$, pore volume: $2.35 \times 10^{-3}$ cc $g^{-1}$) and NCA (0.63 $m^2$ $g^{-1}$, pore volume: $3.12 \times 10^{-3}$ cc $g^{-1}$) cathodes reduces the exposed contact area with the electrolyte, hence improving the cycle performance of the TSFCG cathode. Further study by increasing the upper cutoff voltage (4.4 V) at room temperature and elevated temperature consistently substantiates the superiority of the TSFCG cathode over the CC and NCA cathodes (see Figure S1 in the Supporting Information). To check the long-term cycling performance, pouch-type full cells (25 mAh) using the TSFCG (CC or NCA) cathode and mesocarbon microbead (MCMB) anode were fabricated and cycled between 3.0 and 4.2 V at 25 °C with a constant current rate of 1 C (25 mA). As shown in Figure 3c, compared to the poor capacity retention (71% and 52%, respectively) of the CC and NCA cells, the TSFCG material exhibited outstanding capacity retention of over 88% after 1500 cycles.

Another benefit of the long rod-shaped primary particle morphology, as reported in our previous papers[16] is that

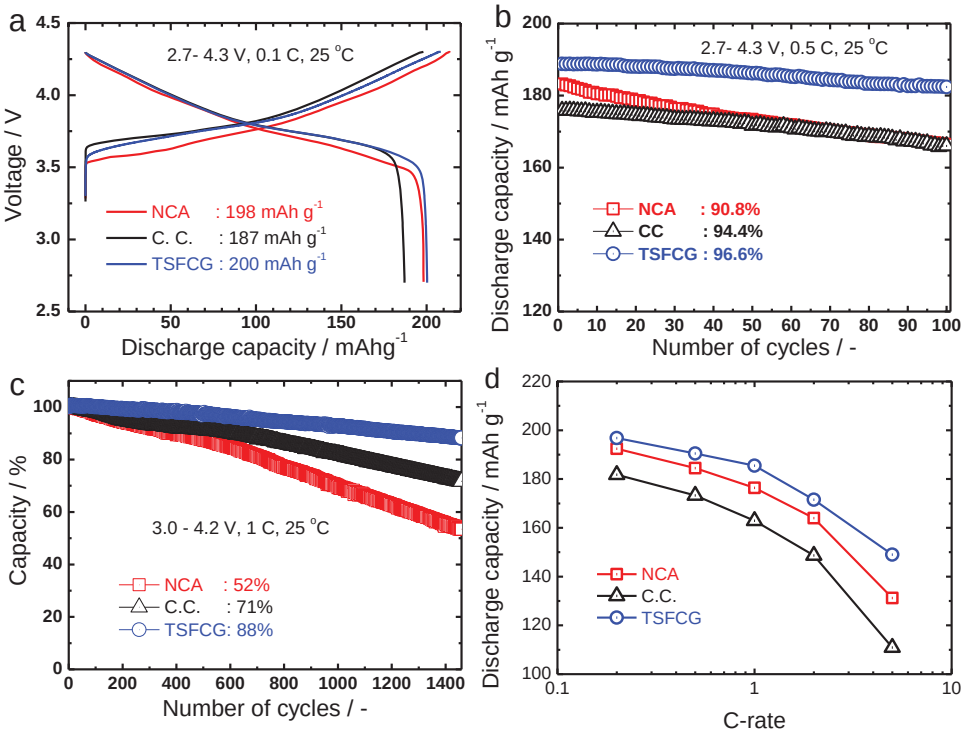


**Figure 3.** Electrochemical performance of CC, NCA, and TSFCG cathodes a) initial charge–discharge curves at 30 °C obtained from a 2032 coin-type half cell using lithium metal as the anode (a current density rate of 0.1 C corresponds to 18 mA $g^{-1}$), b) cycling performance of half cells between 2.7 and 4.3 V at 30 °C by applying a constant current rate of 0.5 C (90 mA $g^{-1}$), c) cycling performance of laminated-pouch-type cell (25 mAh) using MCMB graphite as the anode and CC, NCA, and TSFCG as the cathode at a rate of 1 C, corresponding to 200 mA $g^{-1}$ (upper cutoff voltage of 4.2 V), and d) comparison of rate capabilities of the TSFCG with the CC and NCA cathodes (upper cutoff voltage of 4.3 V versus $Li^+$/Li).

the unique morphology facilitates $Li^+$ diffusion by providing fast diffusion pathways. To validate the fast $Li^+$ ion diffusion through the rod-shaped particles, the chemical $Li^+$ diffusivity for the three cathodes was measured by the galvanostatic intermittent titration technique.[18] The result illustrated that the $Li^+$ diffusivity for the TSFCG cathode ($10^{-10}$ $cm^2$ $s^{-1}$) was almost ten times higher than those of the CC ($10^{-11}$ $cm^2$ $s^{-1}$) and NCA ($10^{-10}$–$10^{-11}$ $cm^2$ $s^{-1}$) cathodes (see **Figure 4**). Therefore, as expected, the TSFCG cathode showed much enhanced rate capability compared to the CC and NCA cathodes (Figure 3d).

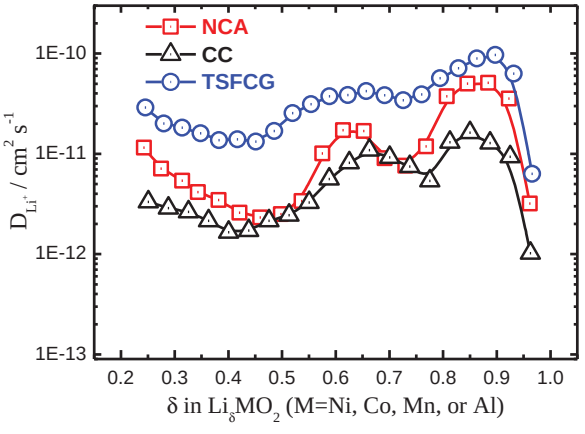


**Figure 4.** Chemical diffusion coefficient, $D_{Li^+}$, of TSFCG, CC, and NCA, as a function of the state of charge.

For example, the capacity retention ratio of the TSFCG cathode at 5 versus 1 C was 75.7%, which is much higher than 68.2% and 61% from the CC and NCA cathodes, respectively.

It is well known that capacity loss on cycling is strongly dependent on the gradual dissolution of transition metal ions from the particle surface, resulting in surface degradation caused by hydrogen fluoride (HF) attack.[19] To measure transition metal dissolution (Ni, Co, and Mn), the active cathode materials were reclaimed from the half-cells charged to 4.3 V and stored in the electrolyte solution at 60 °C for different periods of time. As shown in **Figure 5**, as anticipated, the TSFCG cathode showed the lowest metal dissolution whereas the NCA cathode had the highest metal dissolution. For example, even considering the fact that the Co composition of 0.15 mol% in the NCA cathode is almost equal to 0.12 mol% in the TSFCG and CC cathodes, the Co dissolution in the NCA cathode reached to 3.23 ppm, but was limited to only 0.54 ppm for the TSFCG cathode after 4 weeks. Note that the Mn dissolution from TSFCG is also unexpectedly low compared to the CC cathode even though both cathodes contain identical fraction of Mn. After 4 weeks, the dissolved Mn concentrations for the CC and TSFCG cathodes were 3.14 and 1.24 ppm, respectively. We believe that the lower metal dissolution from the TSFCG cathode was likely due to the unique rod-shape morphology and the low specific area, which is consistent with the electrochemical performances and thermal property (see differential scanning calorimetry (DSC) results: Figure 9).

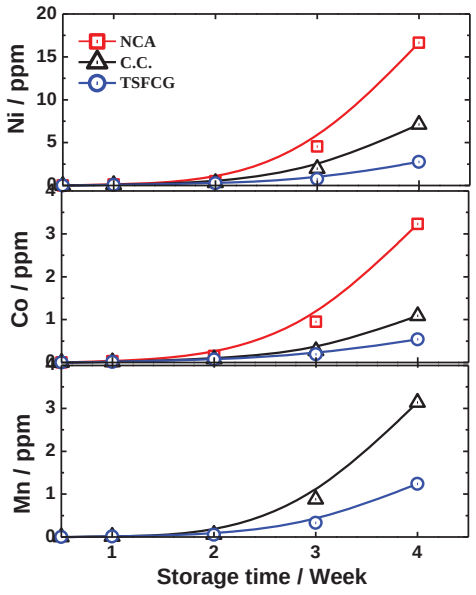


**Figure 5.** Amounts of dissolved Ni, Co, and Mn present after charging the CC, NCA, and TSFCG to 4.3 V versus Li. The electrodes were stored in fresh electrolyte (1 m $LiPF_6$ in EC/EMC = 3:7) at 55 °C for 4 weeks.

To verify the microstructure of the NCA, CC, and TSFCG cathodes after 1500 cycles, TEM analysis of the cycled electrodes was carried out. As expected from the poor capacity retention of the NCA cathodes after 1500 cycles, the TEM images in **Figure 6**a,b for the cycled electrode reveal the active particles that were broken apart and nearly completely pulverized after 1500 cycles. Moreover, due to the severe metal dissolution, the particle surface developed a gear-tooth-like morphology. An electron diffraction pattern in Figure 6c from a single primary particle that was broken off indicates that the layer structure confirmed the 110 zone spot pattern was highly damaged as the electron pattern contained long streaks along 001 direction from the structural defects such as stacking faults. An electron pattern shown in Figure 6d shows the spinel structure indexed to the 111 zone, suggesting that the structural degradation of the NCA electrode during the extended cycling transformed the initial layered structure of the NCA cathode to the spinel phase.

On the other hand, a TEM image of the cycled TSFCG particle verified that the particle remained intact during cycling without any noticeable structural damage at the micrometer level as can be seen in **Figure 7**a. All of the observed TSFCG particles remained stable without pulverization after

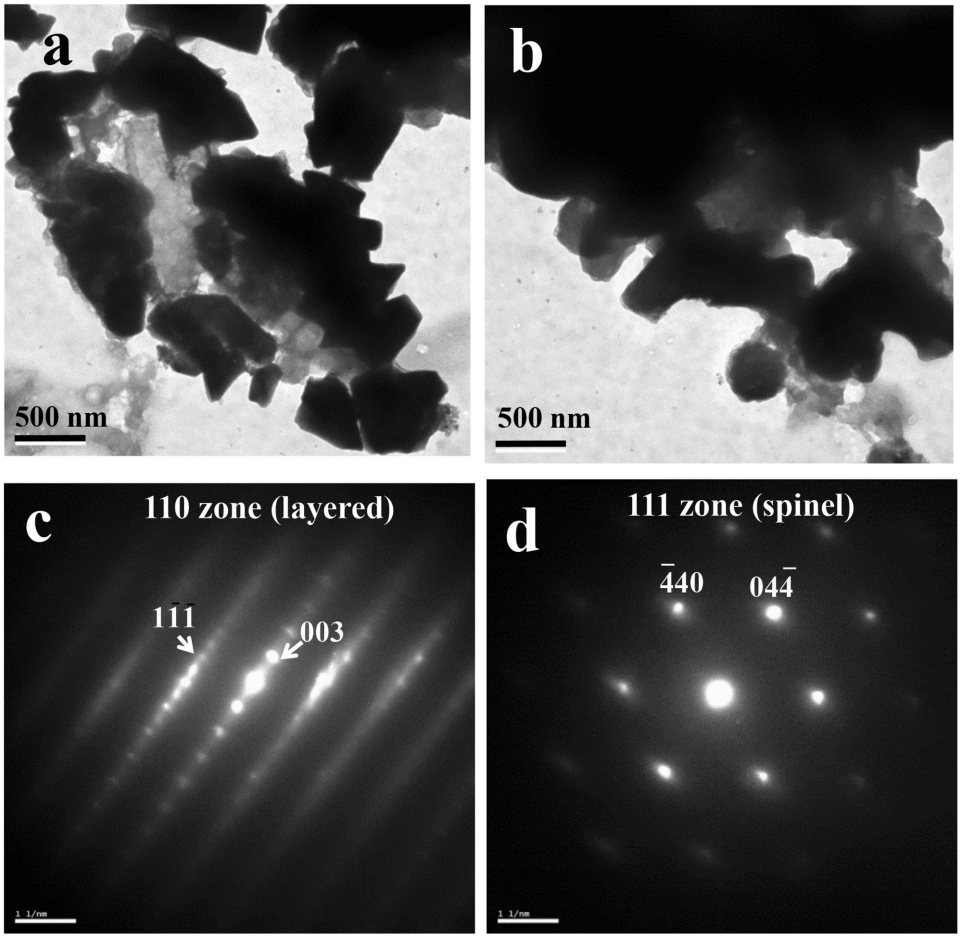


**Figure 6.** a,b) TEM images of the cycled NCA cathode in a pouch-type full cell for 1500 cycles, c) electron diffraction pattern from a primary particle from the cycled NCA cathode in 110 zone of the layered structure, and d) electron diffraction pattern from the cycled NCA cathode, showing 111 zone of the spinel phase.

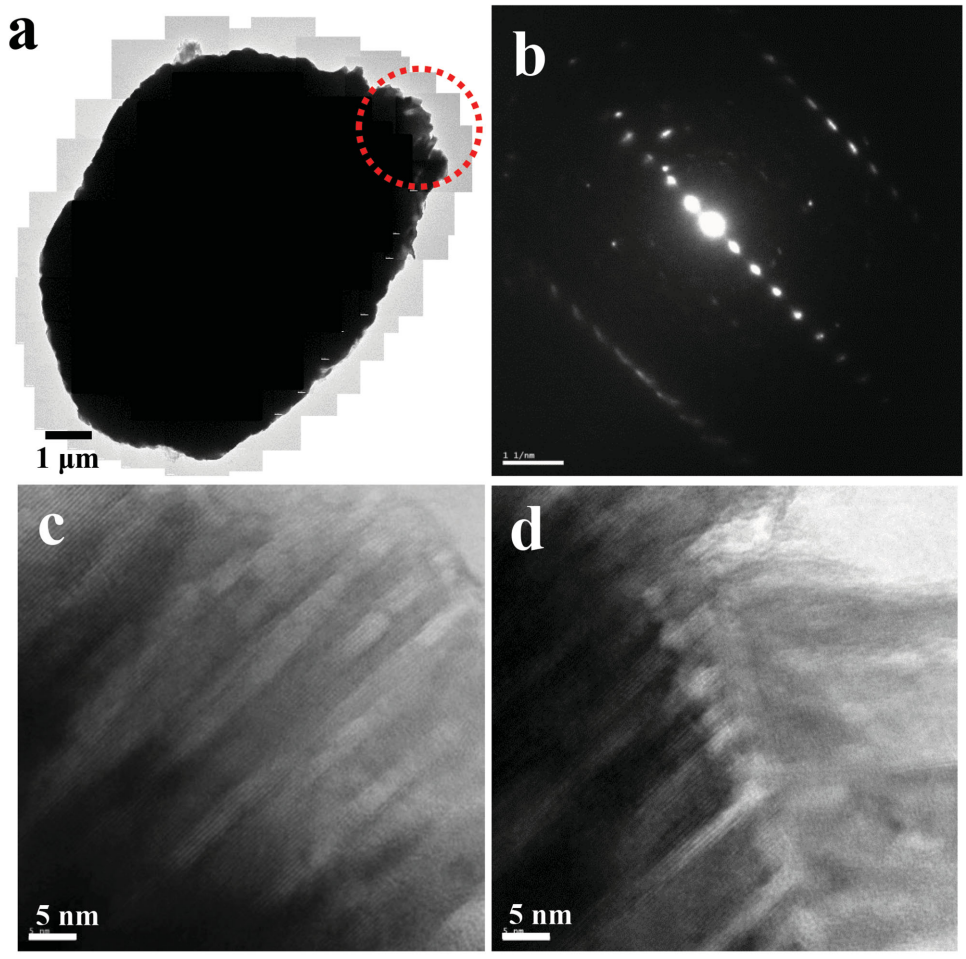


**Figure 7.** a) TEM image of the cycled TSFCG cathode in a pouch-type full cell for 1500 cycles, b) electron diffraction pattern from a primary particle from the cycled TSFCG cathode in –120 zone of the layered structure, and c,d) magnified image of the circled region in (a), illustrating the limited surface damage of the cycled TSFCG cathode.

1500 cycles in agreement with the superior cycle retention of the TSFCG cathode. An electron diffraction pattern from the cycled TSFCG particle shown in Figure 7b was indexed to –120zone of the layered structure. Unlike the diffraction pattern in Figure 6c, the diffraction pattern from the cycled TSFCG particle did not exhibit any streaks. No spinel phase was observed from the cycled TSFCG cathode. Figures 7a,b unequivocally demonstrate that having TSFCG in the cathode helps to maintain the mechanical integrity as well as the structural stability during cycling while achieving the high discharge capacity. Although the surface damage from dissolution of the metal ions was not observed at the micrometer scale from the cycled TSFCG cathode, enlarged high resolution TEM images of the circled region in Figure 7a shows the structural damages incurred during cycling in Figure 7c,d. For the NCA particle, the surface damages were manifest as several hundreds of nanometer-wide gaps on the particle surface whereas the surface damages were limited to a few nanometers for the TSFCG particle. Meanwhile, the structural damages of the cycled CC particle were worse than the TSFCG but better than NCA cathodes in good agreement with the cycle retention data. The cycled CC electrode was broken as shown in **Figure 8**a and at places individual primary particles broken off from the electrode was observed (Figure 8b). An electron diffraction pattern from the circled primary particle shown in Figure 8c was indexed to the 110 zone of the spinel phase. Again, similar to the NCA cathode, the CC cathode likely underwent a series of structural transformations from the layered structure to the spinel phase during cycling, leading to the eventual deterioration of the cycle retention.

Thermal stability of a cathode material is of critical importance to the battery safety. As seen in **Figure 9**, the onset temperature of the exothermal reaction for the NCA cathode was 220 °C with the peak temperature at 234 °C which translates into potential problems for automotive applications. In contrast, the TSFCG cathode shows much improved thermal stability with an exothermic reaction peak at 274 °C and reduced heat generation. Also, the onset temperature shifted to 266 °C which is 46 °C higher than that of the NCA cathode. In agreement with the previously reported FCG-Mn-F material,[16] the TSFCG cathode exhibited better thermal characteristics than the CC cathode by shifting its exothermal reaction to a higher temperatures due to the high thermal stability of the outer surface composition $Li[Ni_{0.60}Co_{0.12}Mn_{0.28}]O_2$ in the TSFCG cathode.

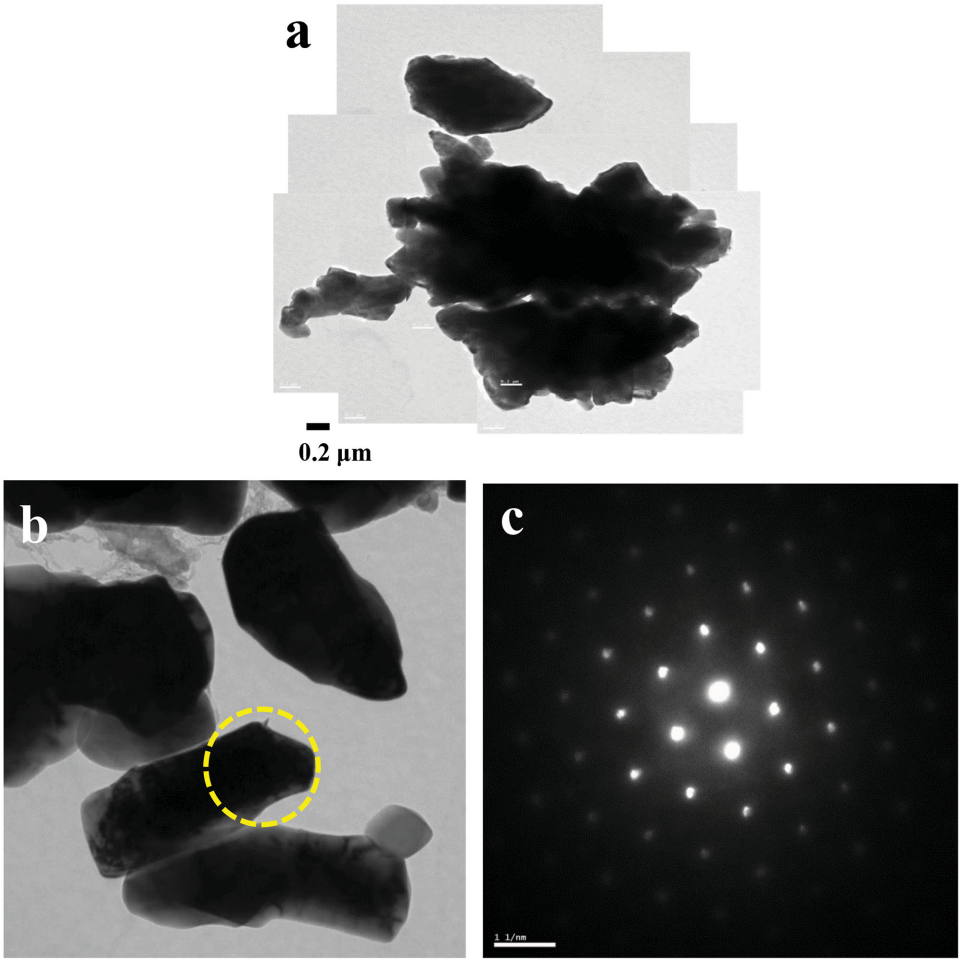


**Figure 8.** a) TEM image of the cycled CC cathode in a pouch-type full cell for 1500 cycles, b) Broken-off primary particles from the cycled CC cathode, and c) electron diffraction pattern from the circled area in (b), indexed to 110 zone of the spinel phase.

## 3. Conclusions

We have developed a novel high-performance $Li[Ni_{0.65}Co_{0.13}Mn_{0.22}]O_2$ cathode material composed of layered lithium transition metal oxide with TSFCG within each particle. This material has been designed to maximize the Ni and Mn content in the inner part of the particle and near the particle surface respectively, resulting in high capacity from the Ni-rich inner part and providing outstanding thermal properties from the Mn-rich outer surface. This material can deliver a reversible discharge capacity of 200 mAh $g^{-1}$ (4.3 V cutoff) with excellent capacity retention of 88% after 1500 cycles in full-cell configuration. Each TSFCG secondary particle consisted of rod-shaped primary particles that radially oriented from the particle center. While the chemical partitioning of the composition generated the observed high capacity and thermal stability, the unique microstructure of the TSFCG secondary particle provided excellent cycle stability and rate capability. TEM analysis of the cycled TSFCG, CC, and NCA cathodes revealed that the TSFCG electrode remained intact with minimal surface deterioration whereas the NCA electrode experienced severe damage during cycling, resulting in pulverization of the particles.

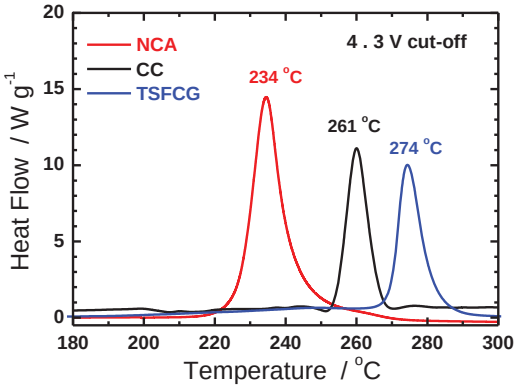


**Figure 9.** Differential scanning calorimetry traces showing heat flow from the reaction of the electrolyte with CC $Li_{1-\delta}[Ni_{0.65}Co_{0.13}Mn_{0.22}]O_2$, TSFCG $Li_{1-\delta}[Ni_{0.65}Co_{0.13}Mn_{0.22}]O_2$, and NCA $Li_{1-\delta}[Ni_{0.8}Co_{0.15}Al_{0.05}]O_2$ charged to 4.3 V.

## 4. Experimental Section

*Synthesis of TSFCG* $Li[Ni_{0.65}Co_{0.13}Mn_{0.22}]O_2$: Spherical TSFCG $[Ni_{0.65}Co_{0.13}Mn_{0.22}](OH)_2$ precursors were synthesized via the

coprecipitation method.[14,15] A Ni-poor aqueous solution consisting of $NiSO_4{\cdot}6H_2O$, $CoSO_4{\cdot}7H_2O$, and $MnSO_4{\cdot}5H_2O$ (molar ratio of Ni:Co:Mn = 68:11:21) from tank 2 was slowly pumped into an Ni-rich (molar ratio of Ni:Co:Mn = 80:5:15) solution in tank 1. Then the homogeneously mixed solution in tank 1 was fed into a batch reactor (40 L) which was filled with a certain amount of deionized water, $NH_4OH$ solution (aq.), and NaOH solution (aq.) in a replenished $N_2$ atmosphere. At the same time, a 4.0 mol $L^{-1}$ NaOH solution (aq.) (molar ratio of sodium hydroxide to transition metal = 2.0) and an $NH_4OH$ chelating agent solution (aq.) (molar ratio of ammonium hydroxide to transition metal = 1.0) were pumped separately into the reactor. During the early stage of the process, $[Ni_{0.80}Co_{0.05}Mn_{0.15}](OH)_2$ (center composition) was coprecipitated first. Nickel–cobalt–manganese hydroxides with different compositions were then gradually piled onto the formed $[Ni_{0.80}Co_{0.05}Mn_{0.15}](OH)_2$ particles to result in a designed composition of Ni, Co, and Mn toward the outer surface of the particles. In order to synthesize TSFCG hydroxide precursor with the second concentration gradient layer, aqueous solution in tank 3 with less Ni concentration (consisting of $NiSO_4{\cdot}6H_2O$, $CoSO_4{\cdot}7H_2O$, and $MnSO_4{\cdot}5H_2O$, molar ratio of Ni:Co:Mn = 51:20:29) was slowly pumped into the mixed solution (molar ratio of Ni:Co:Mn = 70:10:20) in tank 1. The precursor powders were obtained through filtering, washing, and drying at 100 °C overnight. The obtained TSFCG $[Ni_{0.65}Co_{0.13}Mn_{0.22}](OH)_2$ was mixed with $LiOH{\cdot}H_2O$ and the mixture was then calcined at 830 °C for 10 h in oxygen flow.

*Synthesis of Conventional $Li[Ni_{0.65}Co_{0.13}Mn_{0.22}]O_2$ and $Li[Ni_{0.80}Co_{0.15}Al_{0.05}]O_2$*: To synthesize the reference spherical constant-concentration layered oxide cathodes, $NiSO_4{\cdot}6H_2O$, $CoSO_4{\cdot}7H_2O$, and $MnSO_4{\cdot}5H_2O$ (0.65:0.13:0.22, molar ratio for $Li[Ni_{0.65}Co_{0.13}Mn_{0.22}]O_2$ and 0.84:0.16:0.00 molar ratio for $Li[Ni_{0.80}Co_{0.15}Al_{0.05}]O_2$) were used as the starting materials for the coprecipitation process.[20] The obtained $[Ni_{0.65}Co_{0.13}Mn_{0.22}](OH)_2$ hydroxide precursor was mixed with $LiOH{\cdot}H_2O$ (Li/(Ni + Co + Mn) = 1.01 in molar ratio) and calcined at 810 °C for 10 h in oxygen flow for the synthesis of $Li[Ni_{0.65}Co_{0.13}Mn_{0.22}]O_2$. For the synthesis of $Li[Ni_{0.80}Co_{0.15}Al_{0.05}]O_2$, the synthesized $[Ni_{0.84}Co_{0.16}](OH)_2$ hydroxide precursor was mixed with $LiOH{\cdot}H_2O$ and $Al(OH)_3{\cdot}xH_2O$ (Li/(Ni + Co + Al) = 1.01 and Al/(Ni + Co + Al) = 0.05 in molar ratio), and calcined at 750 °C for 10 h in oxygen flow.

*Analytical Techniques*: The chemical composition of the resulting powders was analyzed using AAS (Vario 6, Analytic Jena). The morphology of the powders was determined with scanning electron microscopy (SEM, JSM 6400, JEOL). The morphology of the prepared powders was observed by SEM (JEOL, Model JSM-6340F). To obtain the composition variation of the TSFCG materials, cross sections of the particles were prepared by embedding the particles in an epoxy and grinding them flat. Line scans of the polished surfaces for the prepared TSFCG $Li[Ni_{0.65}Co_{0.13}Mn_{0.22}]O_2$ powders were analyzed via EPMA (SIMADZU, EPMA-1720). TEM samples were prepared by focused ion beam and examined in a JEOL, Model JEM 2100F instrument.

*Electrochemical Test*: For fabrication of the cathodes, the synthesized powders were mixed with carbon black and poly-(vinylidene fluoride) (PVdF) (85:7.5:7.5) in *N*-methylpyrrolidinone. The obtained slurry was coated onto Al foil, vacuum dried and roll pressed. The electrolyte solution was 1.2 M $LiPF_6$ in ethylene carbonate–ethyl methyl carbonate (EC: EMC is 3:7 in volume). Preliminary cell tests were performed with a 2032 coin-type cell using lithium metal as the anode. The cells were charged and discharged by applying a constant current density of 90 mA $g^{-1}$ (0.5 C rate) at 30 and 55 °C in several different cut-off voltage ranges. Long-term cycle-life tests were performed in a laminated-pouch-type full cell (24 mAh). MCMB graphite (Osaka Gas) was used as the anode. The cells were charged and discharged between 3.0 and 4.2 V by applying a constant 1 C current (24 mA corresponds to 180 mA $g^{-1}$) at 25 °C.

*Differential Scanning Calorimetry*: For the DSC experiments, the cells containing the cathode materials were charged at constant voltage of 4.3 V versus Li, and disassembled in an Ar-filled dry box. A 30 µL high-pressure stainless-steel DSC vessel with a gold-plated copper seal was used to host 3–5 mg samples, including solids and electrolyte. The measurements were carried out in a Pyris 1 differential scanning calorimeter (NETZSCH, DSC 200 PC) using a scanning rate of 5 °C $min^{-1}$.

## Supporting Information

Supporting Information is available from the Wiley Online Library or from the author.

## Acknowledgements

This work was mainly supported by the Global Frontier R&D Program (2013M3A6B1078875) on Center for Hybrid Interface Materials (HIM) funded by the Ministry of Science, Information & Communication Technology (ICT) and Future Planning and also supported by the National Research Foundation of Korea (NRF) grant funded by the Korea government Ministryof Education and Science Technology (MEST) (No. 2014R1A2A1A13050479). This work was also financially supported by Bayerische Motoren Werke AG (BMW AG).

Received: April 9, 2015
Revised: May 29, 2015
Published online: June 22, 2015

[1] R. Kostecki, F. McLarnon, *Electrochem. Solid State Lett.* **2004**, *7*, A380.
[2] Y. Itou, Y. Ukyo, *J. Power Sources* **2005**, *146*, 39.
[3] C. H. Chen, J. Liu, M. E. Stoll, G. Henriksen, D. R. Vissers, K. Amine, *J. Power Sources* **2004**, *128*, 278.
[4] http://www.teslamotors.com/ (accessed: June 2015).
[5] J. Shim, R. Kostecki, T. Richardson, X. Song, K. A. Striebel, *J. Power Sources* **2002**, *112*, 222.
[6] S.-H. Lee, C. S. Yoon, K. Amine, Y.-K. Sun, *J. Power Sources* **2013**, *234*, 201.
[7] D. P. Abraham, R. D. Twesten, M. Balasubramanian, I. Petrov, J. McBreen, K. Amine, *Electrochem. Commun.* **2002**, *4*, 620.
[8] R. B. Wright, J. P. Christophersen, C. G. Motloch, J. R. Belt, C. D. Ho, V. S. Battaglia, J. A. Barnes, T. Q. Duong, R. A. Sutula, *J. Power Sources* **2003**, *119–121*, 65.
[9] I. Belharouak, W. Lu, D. Vissers, K. Amine, *Electrochem. Commun.* **2006**, *8*, 329.
[10] J. R. Dahn, E. W. Fuller, M. Obrovac, U. von Sacken, *Solid State Ionics* **1994**, *69*, 265.
[11] H. Arai, S. Okada, Y. Sakurai, J.-I. Yamaki, *J. Electrochem. Soc.* **1997**, *144*, 3117.
[12] W.-S. Yoon, Y. Paik, X.-Q. Yang, M. Balasubramanian, J. McBreen, C. P. Grey, *Electrochem. Solid State Lett.* **2002**, *5*, A263.
[13] Y.-K. Sun, S.-T. Myung, M.-H. Kim, J. Prakash, K. Amine, *J. Am. Chem. Soc.* **2005**, *127*, 13411.
[14] Y.-K. Sun, S.-T. Myung, B.-C. Park, J. Prakash, I. Belharouak, K. Amine, *Nat. Mater.* **2009**, *8*, 320.
[15] Y.-K. Sun, Z. Chen, H.-J. Noh, D.-J. Lee, H.-G. Jung, Y. Ren, S. Wang, C. S. Yoon, S.-T. Myung, K. Amine, *Nat. Mater.* **2012**, *11*, 942.
[16] H.-J. Noh, Z. Chen, C. S. Yoon, J. Lu, K. Amine, Y.-K. Sun, *Chem. Mater.* **2013**, *25*, 2109.
[17] H.-J. Noh, J. W. Ju, Y.-K. Sun, *ChemSusChem* **2014**, *7*, 245.
[18] Y. S. Meng, G. Ceder, C. P. Grey, W.-S. Yoon, M. Jiang, J. Bréger, Y. Shao-Horn, *Chem. Mater.* **2005**, *17*, 2386.
[19] S.-T. Myung, K. Hosoya, S. Komaba, H. Yashiro, Y.-K. Sun, N. Kumagai, *Electrochim. Acta* **2006**, *51*, 5912.
[20] M.-H. Lee, Y.-J. Kang, S.-T. Myung, Y.-K. Sun, *Electrochim. Acta* **2004**, *50*, 939.